HHS Public Access

Author manuscript

Magn Reson Imaging. Author manuscript; available in PMC 2018 June 01.

Published in final edited form as:

Magn Reson Imaging. 2017 June ; 39: 71–81. doi:10.1016/j.mri.2017.01.020.

Biophysical and Neural Basis of Resting State Functional Connectivity: Evidence from Non-human Primates

Li Min Chen[1,2,*], **Pai-Feng Yang**[1,2], **Feng Wang**[1,2], **Arabinda Mishra**[1,2], **Zhaoyue Shi**[1,3], **Ruiqi Wu**[1,2], **Tung-Lin Wu**[1,3], **George H Wilson III**[1,2], **Zhaohua Ding**[1,3,4], and **John C Gore**[1,2,3,*]

[1]Vanderbilt University Institute of Imaging Science, Nashville, TN, 37232, USA

[2]Department of Radiology and Radiological Sciences, Vanderbilt University Medical Center, Nashville, TN, 37232, USA

[3]Department of Biomedical Engineering, Vanderbilt University, Nashville, TN, 37232, USA

[4]Department of Electrical Engineering and Computer Science, Vanderbilt University, Nashville, TN, 37232, USA

Abstract

Functional MRI has evolved from simple observations of regional changes in MRI signals caused by cortical activity induced by a task or stimulus, to the development of task-free acquisitions of time series of images in a resting state. Such resting state signals contain low frequency fluctuations which may be correlated between voxels, and strongly correlated regions are deemed to reflect functional connectivity within synchronized circuits. Resting state functional connectivity (rsFC) measures have been widely adopted by the neuroscience community, and are being used and interpreted as indicators of intrinsic neural circuits and their functional states in a broad range of applications, both basic and clinical. However, there has been relatively little work reported that validates whether inter-regional correlations in resting state fluctuations of MRI (rsfMRI) signals actually measure functional connectivity between brain regions, or to establish how MRI data correlate with other metrics of functional connectivity. In this mini-review, we summarize recent studies of rsFC within mesoscopic scale cortical networks (100μm – 10mm) within a well defined functional region of primary somatosensory cortex (S1), as well as spinal cord and brain white matter in non-human primates, in which we have measured spatial patterns of resting state correlations and validated their interpretation with electrophysiological signals and anatomic connections. Moreover, we emphasize that low frequency correlations are a general feature of neural systems, as evidenced by their presence in spinal cord as well as white matter. These studies demonstrate the valuable role of high field MRI and invasive measurements in an animal model to inform the interpretation of human imaging studies.

[*]Corresponding authors John C. Gore and Li Min Chen, Vanderbilt University Institute of Imaging Science, 1161 21st Avenue South, MCN AA-3109, Nashville, TN, 37232, john.gore@vanderbilt.edu and limin.chen@vanderbilt.edu, Tel: 615 322 8359 (JCG) and 615 9367069 (LMC).

Keywords

monkey; neuroimaging; fMRI; resting state; cortex; spinal cord; white matter

Introduction

Correlations in low frequency blood oxygenation level-dependent (BOLD) signals from different parts of the brain in a resting state were first reported by Biswal et al. (1) and have subsequently become widely adopted as potentially indicating functional connectivity between regions (2, 3). These inter-regional correlations are measurable in the absence of any specific stimulus or task manipulation, though they also may change in the performance of a steady-state task or exercise (4–6) in a manner that can be related to behavioral measures. Correlations in BOLD signals between specific regions of the brain have been proposed to be a key signature of consciously driven mental activity (e.g. see (7–9)). Numerous applications of such measurements in various normal and disease conditions have led to observations of altered resting state networks, such as the so-called large scale ‘default mode network’, in conditions such as schizophrenia and chronic pain (e.g. (10–21)). These observations demonstrate that baseline brain activities are highly relevant for the execution and maintenance of normal brain functions. More importantly, the detection of similar phenomena in very different cortical networks (e.g. oculomotor, sensorimotor, and visual cortices) in anesthetized monkeys (22) has extended this view, suggesting that spontaneous BOLD fluctuations reflect intrinsic synchronous activities within anatomically connected and functionally engaged brain regions. However, despite this high level of interest and multiple potential applications, the validity of inferring direct functional connectivity from resting state fMRI (rsfMRI) data is largely unsubstantiated. Studies in non-human primates which combine fMRI and more invasive measurements have the potential to provide insights into the biophysical basis of resting state signals, and to validate their interpretation and significance. Here we review and summarize some of our recent studies performed at high field in monkeys that aim to better understand the nature and interpretation of resting state functional connectivity (rsFC). Together, they illustrate the value of high field fMRI and invasive studies of animals for informing the interpretation of human rsfMRI acquisitions.

To date, the majority of resting state fMRI studies have examined relatively large-scale networks, involving relatively large volumes of cortex, and much less is known about the characteristics of resting state MRI signals at finer scales. For example, the default mode network has been the focus of numerous studies in which large volumes of cortex have been shown to exhibit variations in their average BOLD signals with other regions that are several centimeters distant. While these larger scale features may be important, the basic processing, functionally homogeneous units of the brain are organized on a much finer, columnar scale. Moreover, execution and maintenance of many brain functions require coordinated activity of brain structures across different scales of brain networks, ranging from macro-scale global networks (in cm to tens of cm, e.g. the default mode network), local meso-scale networks (in hundreds of μm to few mm, e.g. functionally specific digit modules within the primary somatosensory cortex, S1), and micro-scale networks (in μm to tens of μm, at cellular level). At the meso-scale level, modules or columns are believed to be the

fundamental building blocks of cortical specialization, and these often are composed of functionally similar neurons. Individual digit regions in sub-regions of S1 cortex (i.e., areas 3a, 3b, 1 and 2) are classical examples of such modular structures (for reviews, see (23, 24)) and have been the focus of our studies. Such clustered populations of neurons are thought to permit more efficient information processing and functional segregation. In contrast to the many rsfMRI studies of the macro-scale whole brain networks, no reports have focused on the functional organization and connectivity networks at this meso-scale level, partly because of spatial resolution limits imposed on human fMRI studies. As a further step, to validate the idea that rsFC is a more general and intrinsic phenomena within the central nervous system, we have extended our studies from the brain to the grey matter of the spinal cord. By taking advantage of higher signal and contrast to noise ratios at high field (i.e., 9.4T), which in turn allows higher spatial resolution, we have shown that individual digit sub-regions in somatosensory areas exhibit strong rsFC in monkeys (25–28) and this region provides an ideal model for examining basic issues relevant to the interpretation and validation of resting state connectivity. Similarly, as shown below, the sensory and motor horns of spinal cord grey matter also exhibit strong and functionally relevant resting state connectivity, so studies of monkey spine may also shed light on the origins and significance of rsfMRI signals.

Understanding how BOLD signals, which originate from hemodynamic changes, are related to underlying electrical activity is essential for the quantitative interpretation of fMRI data. To date, the majority of studies have focused on understanding the relationships between evoked fMRI signals and underlying electrophysiological changes during the processing of the responses to tasks or stimulations. A number of simultaneous fMRI and single-site micro-electrode recording studies have suggested a direct link between increases in neuronal activity (as quantified by multi-unit activities and local field potentials (LFPs)) and localized increases in cerebral blood flow and BOLD signals in conventional stimulus conditions (e.g. (29–32)), but the precise spatiotemporal correspondence between neural activity and fMRI signals remain rather poorly understood, and there have been very few similar investigations of resting state signals. Our own studies suggest strongly that the spatial extents of rsfMRI and LFP correlations are similar and co-localize, and specific frequency components of spontaneous LFPs underlie correlated rsfMRI signals between regions (33). Studies in monkeys allow the use of invasive multi-channel micro-electrode arrays to record electrophysiological signals from the brain and thus provide unique opportunities for examining quantitatively the relationships between rsfMRI and underlying neural activities.

Distinct from previous work in cats and rodents, the functional regions of the non-human primate brain and spinal cord share considerable homology with humans (34–36). Studies of monkeys provide a crucial linkage between a large existing literature of animal data obtained with invasive methods and human fMRI data involving higher mental functions. The ability to combine very high resolution fMRI, invasive micro-electrode array recordings and histology would be impossible in human subjects. For example, the primary somatosensory cortex S1 provides a unique model for investigating rsfMRI within well defined neural circuits. Nearly all previous sub-millimeter fMRI studies have investigated the visual system, and it is unclear how well the findings can be generalized. The primary somatosensory cortex of squirrel monkey is an alternative experimental model for studies of

functional connectivity, with several advantages. First, the orderly topographic map of S1 serves as an anchor for our understanding of cortical organization. This orderly map is especially reflected in the hand region which is characterized by a lateral to medial representation of individual digits in each of four subregions of areas 3a, 3b, 1 and 2. This has been well established by studies of neuronal receptive field properties and of the effects of preferred stimuli and histological characterizations. Each area has distinct stimulus preferences, suggesting their different roles in specific somatosensory functions. In contrast to the visual system, stimulus evoked activations in the hand region can easily be detected and quantified in 'single condition' maps e.g. vibrotactile stimulation of a single digit, a classical example of the columnar structure of cortex. This eliminates unnecessary ambiguities in designing orthogonal stimuli that are commonly used to reveal modular structures in the visual system. Secondly, we have demonstrated how the functional organization of this region may be mapped at sub-millimeter scale (25–28) for touch processing. Our data have demonstrated that single digit fMRI (both BOLD and CBV) activations can be reliably mapped, their responses scale with the magnitude of the vibrotactile stimuli, they spatially correspond very well with maps revealed with ultra-high resolution optical imaging of intrinsic signals, and confirm that digit activations are organized in a somatotopic manner. Moreover, more recent work has shown that the distinct subregions of S1 show both short-range correlations to other sub-regions within S1 as well as longer range thalamo-cortical connections that can be mapped simultaneously. Additionally the immediately neighboring face area serves as a control region that allows the extent of spatial correlations to be constrained because we know from anatomy that at the 'Hand-Face' border there are very limited cross border lateral intrinsic connections (37–39). This border's unique cytoarchitectonic feature makes it an obvious landmark for identifying and separating hand seed voxels from control face seed voxels in resting state analyses.

In this review, we summarize our resting sate functional connectivity studies of the digit representations in S1 cortex and the monkey cervical spinal cord somatosensory system, in which we have correlated directly, in individual animals, high resolution BOLD and CBV fMRI maps with electrophysiological recordings at meso-scale across digit subregions within S1, along cortical depths, and among spinal grey matter horns.

BOLD rsFC and anatomical connections between digit regions agree closely in areas 3b and 1 of S1

An underlying hypothesis of resting state connectivity analyses is that cortical regions engaged in the same brain function co-activate together and exhibit strong rsFC. To test this, we acquired fMRI activation maps of individual digits to tactile stimulation at moderately high resolution ($0.55\times0.55\times2 = 0.60$ mm^3). We then compared the individual and group average resting state connectivity maps for voxels in e.g. area 3b, with tactile stimulus-evoked activations in the same region. The stimulation evoked activation pattern for a single digit (Fig. 1) has islands of activation in different sub-regions and is very similar to the resting state connectivity maps of seed voxels placed in the same digit regions in areas 3b and 1. The inter-areal correlations for a single digit were stronger than within-area correlations to other digits. The similarity between resting state connectivity maps and

tactile stimulus driven activation patterns suggests that cortical regions that have the same stimulus preference also have strong resting state connectivity. Importantly, the activation maps were confirmed with subsequent electrophysiological recordings (28), and a close examination showed pair-wise highly correlated voxels were located at topographically appropriate regions. Anatomical DBA tracer injected into the digit location in area 3b revealed dense, intrinsic cortico-cortical connections in the corresponding digit location in area 1 (data not shown; see (28)). These studies confirmed there is a close spatial correspondence between strong rsFC and dense anatomical connections, and provide strong evidence for a direct relationship between fine-scale functional connectivity metrics from rsfMRI with electrical and anatomical connections at this scale in this system (28).

Inter-areal rsfMRI connectivity strength co-varies with inter-areal coherence of LFPs between areas 3b and 1 of S1

Previous studies in monkey visual cortex and rats have identified temporally correlated fluctuations of gamma band LFPs and low frequency fluctuations of rsfMRI signals (e.g. (40)) at single recording sites. No previous studies, however, have directly related the inter-regional differences in the rsfMRI and LFP correlations between two functionally related cortical regions within a small cortical circuit. We tested the hypothesis that correlations in specific frequency components of spontaneous LFPs underlie correlated low frequency fluctuations of rsfMRI signals between regions. We compared directly the strengths of inter-regional connectivity between digit regions (e.g. area 3b digit 3 to- area 1 digit 3) versus digit-face (area 3b digit 3 – area 3b face region) as measured by rsfMRI correlations versus coherence of spontaneous LFPs in the same regions on the same animal. We found that digit-digit rsfMRI connectivity was significantly stronger than digit-face connectivity. Spontaneous LFP signals of all frequency bands except theta showed the same inter-regional connectivity differences. Figure 2 shows the results for rsfMRI and the Delta band LPF signals. This study thus demonstrated the existence of correlated and differentiable functional connectivity within a local fine-scale network of primary somatosensory areas sub-regions (hand and face regions in areas 3b and 1) detectable with both rsfMRI and LFPs (33).

High spatial correspondences between BOLD and LFP metrics in both stimulation and resting states

Columns are the building blocks of cortical function. By directly comparing 2D distributions (the Point Spread Function, PSF) of BOLD and LFP signals in both stimulation and resting states, we found that BOLD signal changes raised within a single digit representation column aligned spatially very well with LFP signals in response to tactile stimulation. Resting state BOLD fMRI and LFP signals also exhibited very similar inter-voxel spatial correlation profiles. These findings indicate that at columnar level BOLD signals faithfully reflect underlying neuronal activity during both information processing and at rest. Neurons engaged in the same brain function exhibit a high degree of synchronized signal fluctuations at rest.

We quantified the PSF or intrinsic spatial spread of imaging signals since it sets the theoretical limits on spatial resolution of functional mapping. The PSF of BOLD signals has been previously measured in the visual cortex of humans and animals (41), but no study has compared directly the spatial extents of the hemodynamic BOLD signal and underlying neural electrophysiological activity, nor the local (intra-regional) extents of resting state correlations in either modality. There also remains uncertainty about the relative importance of the intrinsic extent of activity, the effects of hemodynamic blurring or technical acquisition parameters such as voxel size on the observed extent of BOLD signals. We quantified the PSFs of BOLD activations to subtle vibrotactile stimuli and their corresponding resting state correlations and compared them with those of LFPs, which were characterized using two 7×7 microelectrode array (98-channels in total) placed in the same positions in cortex (42). We found that the BOLD and LFP responses to tactile stimuli were both roughly elliptical and elongated along the digit-to-digit direction (medial to lateral) in area 3b, but not so in area 1 (Fig. 3). Importantly, in both areas, PSFs of BOLD and LFP for both activation and resting state correlations were in close agreement. These observations for the first time demonstrate that the spatial distributions of BOLD signals not only directly reflect the area of the underlying LFP, but also their spatial correlations are near identical. The PSFs for both BOLD and LFP were about 1 mm, demonstrating that the hemodynamic blurring of neural activity in BOLD images need not be a limiting effect in practice. The PSFs of resting state BOLD and LFP are about 1.3 times broader than those of stimulus-evoked responses. These results are the first demonstrations of the ability of BOLD and LFP to map and differentiate sub-millimeter scale cortical modular structures and their local connectivity (42).

High resolution rsfMRI shows differences in functional connectivity with cortical depth between sub-regions of S1

Cerebral cortex exhibits a laminar structure, and the variation of neural activity with cortical depth is an important aspect of the functional organization of the brain. Within each functional module, information is processed across multiple cortical layers. For example, the six horizontal laminae are often grouped into three classes of neurons: supra-granular layers (I–III), a granular layer (IV), and two infra-granular layers (V–VI). The functions of each layer are distinct. Of the supra-granular layers (I–III), layer III receives input from other cortical columns, and cells in layers II and III project to other parts of the cortex. The granular layer (IV) receives inputs from the thalamus and sends signals to the rest of the column (primarily up to layers II and III). Intra-granular layers (V–VI) receive input from the supra-granular cells of adjacent columns, and send signals mainly to extra-cortical structures (e.g., thalamus and other subcortical structures). Thus, because the anatomical connections between layers are well established, examination of the functional connectivity between layers of functionally related regions provide insights into local information flow (e.g., feedback or feedforward) for specific functions. Alterations in laminar level connectivity have been linked to developmental and mental disorders (e.g. (43)). However, to date there have been only a few rsfMRI studies that have investigated the differential patterns of connectivity within and between layers (44–46). We examined the laminar (across cortical depths) functional connectivity between areas 3b and 1 of S1 cortex using

stimulus-driven and resting state fMRI (BOLD and CBV) acquisitions at different sub-millimeter resolutions. FMRI activation maps generated by tactile stimulation of individual digits were again used to precisely localize functional regions and guide the selection of seed voxels. We detected reproducible stimulus-evoked BOLD and CBV signal changes in areas 3b and 1 in all animals studied. BOLD activation foci were located in the superficial section (or layer) (33% of the cortical length) whereas CBV activation foci were located in the middle section (51%) of areas 3b. The distance between BOLD and CBV activation foci was ~0.8 mm; the mean thickness of area 3b was ~2.3 mm. Pair-wise functional connectivity analysis was performed between layer pairs of areas 3b and 1. Resting state BOLD signals showed strong functional connections between superficial (I–III) and middle (IV) layers. In contrast, resting state CBV signals revealed strong functional connectivity between middle (IV) and deeper (V–VI) layers (Fig. 4). Thus it is clear that both resting state BOLD and CBV signals are sensitive to detecting layer-specific intrinsic functional connections between areas 3b and 1, but the specific inter-layer connectivity patterns of resting state BOLD and CBV signals differ. These differences likely partially reflect differences in the detailed vasculature of these different layers (47) as well as the strength of neural baseline connectivity. It is noted that the three different layers we refer to are estimated, so they do not directly correspond to the specific I–VI layers that can be specified with histological evaluation of the tissue sections.

Apparent temporal dynamic changes in resting-state connectivity in somatosensory cortex

While resting state correlations by definition connote that neural synchrony (as measured by BOLD signal fluctuations) is statistically stationary, recent work has suggested brain circuits may change between states over different time scales (48). Variations over time in the estimated resting-state correlations between BOLD signals from different cortical areas may therefore indicate changes in brain states and functional connectivity. However, apparent variations over time may also arise from stationary signals when the sample duration is finite. There has recently been considerable interest in understanding the nature and significance of these dynamic changes in connectivity. For example, a vector autoregressive (VAR) null model was proposed to simulate rsfMRI data, which provides a stationary model for identifying possible temporal dynamic changes in functional connectivity (49). Resting state acquisitions from the sub-regions of S1 of monkey brain provide an invaluable set of data to test such models. When applied to our data from S1 of monkey brain, the VAR model does not replicate important features of the real measurements. We therefore proposed an alternative, simpler model that uses a filtered stationary dataset which generates statistically stationary time series from random data with a single prescribed average correlation coefficient (50). In addition, we investigated a non-stationary model to see if it is better able to replicate dynamic changes in real fMRI connectivity data obtained from monkeys. We compared simulated results using these three models with the behaviors of the primary somatosensory cortex networks in anesthetized squirrel monkeys using a sliding window correlation analysis and a rigorous Kolgomorov-Smirnov statistical approach for assessing similarity of features of the dynamic correlations. We found that at short window sizes, both stationary models reproduced the distribution of correlations of real signals well, but they

failed at longer window sizes, and a dynamic model was needed to reproduce the behavior of correlations between real signals. While stationary models replicate several features of real data, a close representation of the behavior of resting state data acquired from somatosensory cortex of non-human primates is obtained only when a non-stationary or underlying dynamic correlation is introduced, suggesting dynamic variations in connectivity are real and deserve further study (50).

Mild and non-selective effects of isoflurane on inter-regional rsFC

Anesthesia is essential for obtaining high resolution fMRI data in animals because it reduces motion and physiological artifacts. However, there are potential concerns about possible suppressive effects of the anesthetic, which may confound observations of neural activity. To evaluate to what extent isoflurane affects resting state fMRI signals, we performed dose-dependent studies as three levels of isoflurane were administered. The choices of these three levels of anesthesia were based on two key observations, that both robust neuron electrophysiological activity and robust stimulus-evoked and resting state fMRI signals could be detected. For example, under 0.875% isoflurane, we observed significantly stronger inter-areal digit-digit functional connectivity than for digit-control (face) correlations. When the anesthesia level was increased to 1.25% or reduced to 0.5%, the differences between digit-digit and digit-face correlations were sustained even as the mean power of signal fluctuations changed (Fig. 5). Together, these observations give us confidence that under light anesthesia, inter-areal functional connectivity differences are preserved in conditions under which robust neural activity is still present. Moreover, they confirm that resting state signals are related to underlying baseline neural activity. Anesthesia introduced mild non-specific suppressive effects, but did not introduce area selective effects (51).

Detection of distinct fMRI responses in spinal cord to noxious heat and innocuous touch stimulation

Prior to acquiring resting state signals, we first demonstrated and compared the horn-horn fMRI activation patterns of tactile versus nociceptive stimuli. Figure 6 shows that tactile or nociceptive heat stimulation of the same pair of digits (D2 and D3) evoked different fMRI responses (in magnitudes) across the four horns. With 8 Hz tactile stimulation, the strongest signal change was detected in the ipsilateral dorsal horn, whereas contralateral and ipsilateral ventral horns showed much weaker signal changes. As a control, white matter showed no significant changes. By contrast, noxious heat stimulation of the same pair of digits elicited equally stronger responses in bilateral dorsal horns and ipsilateral ventral horn (Fig. 6). Time courses showed that contralateral dorsal and ventral horns exhibited the most selective responses to heat versus tactile stimuli respectively (Fig. 7). These results highlight the fact that the overall cross-horn activation patterns to tactile and nociceptive heat inputs are more complex than have previously been recognized. Instead of functioning as a simple motor output horn, ventral horns (primarily ipsilateral) are also engaged in the processing of both tactile and nociceptive inputs (52). This finding is significant because the ventral horn activation to unilateral painful stimuli may be explained by the engagement of local spinal

reflex circuitry, but the similar responses to innocuous tactile stimuli suggest that the ventral horn likely plays a larger role than just mediating simple pain-signal reflex activity (53).

Resting state functional connectivity (rsFC) networks in spinal cord

The identification of patterns of highly correlated low frequency MRI signals in the resting state has clearly and dramatically influenced our view about the functional organization of the brain, and potentially provides a powerful approach to delineate and describe cortical circuits. To date, over 6000 studies have been reported that use rsfMRI to detect and characterize functional connectivity. However, whether resting state fluctuations are a general feature of neural systems has not previously been explored, and to date there have been only two conclusive investigations of functional connectivity within the grey matter of the human spinal cord. We published our findings that in a resting state, BOLD signals within spinal cord grey matter in the human spinal cord do exhibit significant fluctuations that are correlated between ventral (motor) horns and between dorsal (sensory) horns, corresponding to motor and sensory networks (54). Subsequently, Kong et al. (55) published similar findings. The fact that the spinal cord motor network was identified in both papers despite different data analyses and methods of acquisition adds credibility to this discovery.

These highly exciting and provocative results are currently being explored in clinical applications. Moreover, as emphasized above, although resting state correlations are already being widely used to assess functional connectivity in the brain, their precise interpretation remains unclear, and their biophysical basis as direct indicators of functional connectivity is unsubstantiated. This is even more the case in the spine, where we have much less knowledge of the detailed vascular physiology or organization of specific within-segment horn-to-horn functional neural circuits. Again, studies at high field and high spatial resolution in non-human primates allows detailed investigation of the nature and significance of spinal cord signals.

Quantification of functional connectivity between horns within the spinal cord

With the identification of stimulus-responsive voxels, we next tested their functional connectivity by quantifying the correlation coefficients of the resting state fMRI signals from voxels or small ROIs in all four spinal horns and adjacent control white matter (53). When a seed voxel was placed in the left ventral horn in the third slice (Fig. 8A), we observed a widespread functional connectivity pattern to other horns both within and across image slices. This pattern is very similar to the activation pattern evoked by tactile stimuli (Fig. 6A). Importantly, using data driven ICA analysis of resting state fMRI signals, we identified a similar but not identical intrinsic connectivity network (data not shown).

Weakened inter-horn functional connectivity recoveries over time after traumatic injury

Studies in non-human primates allow interventions and perturbations of normal neural functions to be used to probe the meaning of rsfMRI correlations. To understand the

functional and behavioral relevance of the rsFC within spinal cord grey matter, we further examined whether and how traumatic injury affects the functional connectivity among horns of the spinal cord. We started our study with a simple and well-established spinal cord injury model of a dorsal column lesion (DCL) that selectively disrupts ascending afferents that carry discriminative tactile information from body to brain, and causes temporary loss of the functional integrity of the spine (56, 57). Compared to other models of spinal cord injury (SCI), DCL of the cervical spinal cord has several advantages. First, DCL at a high cervical level (C4–C6) in monkeys exclusively disrupts the afferent fiber bundle carrying cutaneous tactile information from hand to brain while preserving descending motor pathways, temperature, pain, and crude touch. DCL therefore causes a behavioral impairment in hand use with little confounding influence from motor function deficits. This impairment recovers over a period of a few months following the injury, allowing longitudinal studies (58–60). The neighboring input intact spinal segments (e.g. above lesion site) serve as an ideal 'built-in' control for evaluating changes in spinal rsFC. More importantly, the precise projection pattern of digit afferents to the up-stream cuneate nucleus allows accurate quantification of the afferent disruption. Moreover, there are reliable tracer techniques available to identify and separate deafferented digits and to quantify the extent of the injury. With this information, the extent and levels of spinal cord injury can be quantitatively characterized and ultimately correlated with functional and behavioral changes.

After introducing unilateral lesions at the C5 level (entering zone for D2/D3 afferents), we found that the correlations between horn-to-horn pairs in the slices below the injuries were significantly weakened immediately after injury compared to those corresponding ROI pairs above-the lesion (see Figure 9). Figure 9 shows that after unilateral injury to the spinal cord, rsFC changes are specific to the side of the lesion and occur in spinal cord segments below the injury. We therefore propose that rsFC can be used as a non-invasive imaging biomarker of spinal functional integrity (for detailed discussions see (53)). From a clinical translational point of view, a good biomarker is expected to have enough sensitivity and specificity to indicate changes in individual subjects. Our preliminary results show inter-horn functional connectivity changes over time after injury (Fig. 9). Dorsal-dorsal horn connections exhibited a consistent recovery trend (increased correlation r values at subsequent time points). Thus, resting state correlations are detectable in the spinal cord and the strength of inter-horn rsFC correlates with the integrity of spinal cord function during recovery from injury. RsFC measures may therefore be used to detect and quantify functional circuit changes in individual subjects.

Behavioral deficits on food reaching and retrieval task correlate with severity of SCI

The practical significance of rsFC measurements depends on whether they reflect neural function and behavior. In the DCL model of SCI described above, appropriate tasks and behavioral analyses provide sensitive behavioral/functional correlates of the effects of deafferentation and subsequent reorganization in monkeys (59, 61). A particularly sensitive test relevant to our injury model in monkeys is performance on a food reaching and retrieval task, measured by the total success rate and number of digit flexions per success from four

wells of increasing depth containing food. Hand use performance may be assessed using several parameters derived from high-speed video recording of reaching and retrieval behaviors of awake monkeys after they are injured and as they recover. Typically, success rate drops and digit flexions/success increase one-week post-lesion, but show more significant recovery at 2 and 3 weeks, consistent with neural plastic adaptations during this period (62). A key observation has been that the extent of the behavioral deficit in this particular task is correlated with the level and extent of the spinal cord lesion and the degree of cortical remodeling. Moreover, the pattern of behavioral recovery can be directly related to the time course of changes in the rsFC measures in the cord obtained from MRI.

Resting state correlations are detectable in white matter and are anisotropic

The vast majority of fMRI studies have been focused on brain grey matter and there has been only a very limited number of reports of corresponding changes in white matter (63–68). The dearth of fMRI literature on white matter is conventionally attributed to an absence of significant hemodynamic changes within white matter in response to changes in electrical activity, so that any corresponding weak BOLD signals are not reliably detectable by current means. Most investigators have failed to show convincing evidence for focal activation in white matter following a task or stimulus, so the field of fMRI has evolved to almost completely disregard BOLD effects in white matter. Compared to grey matter, white matter is irrigated by much less dense vasculature (69, 70), with blood flow approximately one-fourth of that in the grey matter (71). Even if BOLD changes occur, they may be proportionally reduced, and thus demand higher sensitivity for detection. Despite the four-fold reduction in blood flow, the oxygen extraction fraction is relatively uniform in the resting brain (71). We have observed that variations in T2* weighted MRI signals in a resting state show comparable intensity and temporal variability profiles in both white and grey matter. The voxel-averaged temporal variations of MRI signals in white matter are ~80% those in grey matter (72); analysis of the power spectra of BOLD signals from both white matter and grey matter shows that the ratio of signal power in the low frequency range of 0.01 to 0.08 Hz to total variance are comparable (72, 73). These indicate that resting state variations that potentially reflect neural activity in grey matter may also be detectable in white matter. Moreover, inter-voxel correlations of resting state signal from white matter show spatial anisotropy and reveal distinct underlying structures (72, 73). Thus it appears that appropriate analysis of resting state acquisitions may reveal signal variations within white matter that directly reflect functional activity.

The finding the inter-voxel correlations in resting state BOLD signals from white matter show a degree of spatial anisotropy forms the basis of our proposal to construct functional tensor maps from spatio-temporal analyses of BOLD signals (72). In our early studies, series of resting state MR images were acquired from human subjects at 3T using single shot echo planar imaging, just as used for regular fMRI acquisitions, and from these data functional tensors were constructed, but again the non-human primate brain provides an excellent animal model in which to investigate BOLD changes in white matter more closely. Figure 10 confirms that anisotropic resting state correlations occur in the white matter of monkey

brain, just as for humans, and illustrates the underlying structure revealed by constructing functional tensors. Figure 10 shows histograms of the fractional anisotropy of the functional tensors from within segmented volumes of white and grey matter, showing that the degree of anisotropy in white matter much exceeds anything detectable in grey matter. These high correlations appear to extend over long distances but are confined to specific structures, signifying there are synchronized temporal variations tied to these structures. Further examination of functional and diffusion tensor maps show that, in grey matter regions, both functional and diffusion tensors appear isotropic except at the boundaries. In white matter, both tensors are more elongated and gross agreement between the functional and diffusion tensors can often be observed in several regions.

Just as for grey matter, we aimed to assess whether MRI signal fluctuations in white matter vary for different baseline levels of neural activity. We performed imaging studies on live squirrel monkeys under different levels of isoflurane anesthesia at 9.4T (74). We found 1) the fractional power (0.01–0.08Hz) in white matter was between 60 to 75% of the level in grey matter; 2) the power in both grey and white matter low frequencies decreased monotonically in similar manner with increasing levels of anesthesia; 3) the distribution of fractional anisotropy values of the functional tensors in white matter were significantly higher than those in grey matter; and 4) the functional tensor eigenvalues decreased with increasing level of anesthesia. Our results suggest that as anesthesia level changes baseline neural activity, white matter signal fluctuations behave similarly to those in grey matter, and functional tensors in white matter are affected in parallel (74).

Summary and Conclusions

There are several important yet unanswered questions regarding the interpretation of resting state fMRI signals that are already in widespread use, and which potentially can provide uniquely valuable information on the functional architecture of the brain. Resting state correlations in MRI signals are interpreted as measures of functional connectivity, yet there have been very few substantive studies that validate this interpretation. The studies described above were undertaken with the goal of relating fMRI metrics of connectivity directly to invasive, “gold standard” measurements in non-human primates with a greater sensitivity and spatial resolution than possible in human subjects. In addition, these studies have revealed new information on the functional organization and inter-layer relationships within a well defined neural system in the primate brain which is directly comparable to human brain organization. Overall, such studies are uniquely valuable for informing human fMRI brain studies. The use of higher field strengths emphasizes microvascular BOLD effects more strongly than at lower field, and thus the fidelity of brain mapping can be expected to be more accurate. The increased contrast to noise enables higher, sub-millimeter resolution imaging to be performed, which reduces partial volume effects and increases the ability to locate and separate fine-grained activity. The use of mild anesthesia does not seem to reduce the detectability of functional and neural activity signals but ensures a reduction in physiological noise and motion. Most importantly, the use of animals allows invasive measurements of LFPs that can be correlated with fMRI, and the introduction of controlled perturbations such as a spinal cord injury to modulate neural responses. The use of

appropriate animal models is thus crucial to advancing our understanding of the biophysical basis and significance of resting state and other functional MRI signals.

Acknowledgments

These studies are supported by a Dana Foundation and a National Institutes of Health Grant RO1 NS069909 to LMC, RO1 NS093669 and RO1 NS078680 to JCG, and RO1 NS092961 to JCG/LMC. We thank Chaohui Tang for her technical support on animal preparation, Fuxue Xing for his assistance on fMRI data collection.

References

1. Biswal B, Yetkin FZ, Haughton VM, Hyde JS. Functional connectivity in the motor cortex of resting human brain using echo-planar MRI. Magn Reson Med. 1995; 34(4):537–41. [PubMed: 8524021]
2. Greicius MD, Krasnow B, Reiss AL, Menon V. Functional connectivity in the resting brain: a network analysis of the default mode hypothesis. Proc Natl Acad Sci U S A. 2003; 100(1):253–8. [PubMed: 12506194]
3. Guye M, Bartolomei F, Ranjeva JP. Imaging structural and functional connectivity: towards a unified definition of human brain organization? Curr Opin Neurol. 2008; 21(4):393–403. [PubMed: 18607198]
4. Hampson M, Driesen NR, Skudlarski P, Gore JC, Constable RT. Brain connectivity related to working memory performance. J Neurosci. 2006; 26(51):13338–43. [PubMed: 17182784]
5. Newton AT, Morgan VL, Gore JC. Task demand modulation of steady-state functional connectivity to primary motor cortex. Hum Brain Mapp. 2007; 28(7):663–72. [PubMed: 17080441]
6. Newton AT, Morgan VL, Rogers BP, Gore JC. Modulation of steady state functional connectivity in the default mode and working memory networks by cognitive load. Hum Brain Mapp. 2011; 32(10): 1649–59. [PubMed: 21077136]
7. Fingelkurts AA, Kahkonen S. Functional connectivity in the brain–is it an elusive concept? Neurosci Biobehav Rev. 2005; 28(8):827–36. [PubMed: 15642624]
8. Fox MD, Raichle ME. Spontaneous fluctuations in brain activity observed with functional magnetic resonance imaging. Nat Rev Neurosci. 2007; 8(9):700–11. [PubMed: 17704812]
9. Rogers BP, Morgan VL, Newton AT, Gore JC. Assessing functional connectivity in the human brain by fMRI. Magn Reson Imaging. 2007; 25(10):1347–57. [PubMed: 17499467]
10. Liao W, Zhang Z, Pan Z, Mantini D, Ding J, Duan X, et al. Altered functional connectivity and small-world in mesial temporal lobe epilepsy. PLoS One. 5(1):e8525. [PubMed: 20072616]
11. Honey GD, Suckling J, Zelaya F, Long C, Routledge C, Jackson S, et al. Dopaminergic drug effects on physiological connectivity in a human cortico-striato-thalamic system. Brain. 2003; 126:1767–81. [PubMed: 12805106]
12. Baliki MN, Chialvo DR, Geha PY, Levy RM, Harden RN, Parrish TB, et al. Chronic pain and the emotional brain: Specific brain activity associated with spontaneous fluctuations of intensity of chronic back pain. J Neurosci. 2006; 26(47):12165–73. [PubMed: 17122041]
13. Garrity AG, Pearlson GD, McKiernan K, Lloyd D, Kiehl KA, Calhoun VD. Aberrant “default mode” functional connectivity in schizophrenia. Am J Psychiatry. 2007; 164(3):450–7. [PubMed: 17329470]
14. Baliki MN, Geha PY, Apkarian AV, Chialvo DR. Beyond feeling: Chronic pain hurts the brain, disrupting the default-mode network dynamics. J Neurosci. 2008; 28(6):1398–403. [PubMed: 18256259]
15. Camchong J, Macdonald AW 3rd, Bell C, Mueller BA, Lim KO. Altered Functional and Anatomical Connectivity in Schizophrenia. Schizophr Bull. 2009
16. Cao X, Cao Q, Long X, Sun L, Sui M, Zhu C, et al. Abnormal resting-state functional connectivity patterns of the putamen in medication-naive children with attention deficit hyperactivity disorder. Brain Res. 2009; 1303:195–206. [PubMed: 19699190]
17. Monk CS, Peltier SJ, Wiggins JL, Weng SJ, Carrasco M, Risi S, et al. Abnormalities of intrinsic functional connectivity in autism spectrum disorders. Neuroimage. 2009; 47(2):764–72. [PubMed: 19409498]

18. Assaf M, Jagannathan K, Calhoun VD, Miller L, Stevens MC, Sahl R, et al. Abnormal functional connectivity of default mode sub-networks in autism spectrum disorder patients. Neuroimage. 2010; 53(1):247–56. [PubMed: 20621638]
19. Cubillo A, Halari R, Ecker C, Giampietro V, Taylor E, Rubia K. Reduced activation and inter-regional functional connectivity of fronto-striatal networks in adults with childhood Attention-Deficit Hyperactivity Disorder (ADHD) and persisting symptoms during tasks of motor inhibition and cognitive switching. J Psychiatr Res. 2010; 44(10):629–39. [PubMed: 20060129]
20. Henseler I, Falkai P, Gruber O. Disturbed functional connectivity within brain networks subserving domain-specific subcomponents of working memory in schizophrenia: Relation to performance and clinical symptoms. J Psychiatr Res. 2010; 44(6):364–72. [PubMed: 19837416]
21. Liao W, Chen HF, Feng YA, Mantini D, Gentili C, Pan ZY, et al. Selective aberrant functional connectivity of resting state networks in social anxiety disorder. Neuroimage. 2010; 52(4):1549–58. [PubMed: 20470894]
22. Vincent JL, Patel GH, Fox MD, Snyder AZ, Baker JT, Van Essen DC, et al. Intrinsic functional architecture in the anaesthetized monkey brain. Nature. 2007; 447(7140):83–6. [PubMed: 17476267]
23. Mountcastle VB. The columnar organization of the neocortex. Brain. 1997; 120(Pt 4):701–22. [PubMed: 9153131]
24. Thomson AM, Bannister AP. Interlaminar connections in the neocortex. Cereb Cortex. 2003; 13(1):5–14. [PubMed: 12466210]
25. Chen LM, Turner GH, Friedman RM, Zhang N, Gore JC, Roe AW, et al. High-resolution maps of real and illusory tactile activation in primary somatosensory cortex in individual monkeys with functional magnetic resonance imaging and optical imaging. J Neurosci. 2007; 27(34):9181–91. [PubMed: 17715354]
26. Zhang N, Gore JC, Chen LM, Avison MJ. Dependence of BOLD signal change on tactile stimulus intensity in SI of primates. Magn Reson Imaging. 2007; 25(6):784–94. [PubMed: 17614230]
27. Chen L, Mishra A, Newton AT, Morgan VL, Stringer EA, Rogers BP, et al. Finescale functional connectivity in somatosensory cortex revealed by high-resolution fMRI. Magn Reson Imaging. 2011; 29(10):1330–7. [PubMed: 21982165]
28. Wang Z, Chen LM, Negyessy L, Friedman RM, Mishra A, Gore JC, et al. The Relationship of Anatomical and Functional Connectivity to Resting-State Connectivity in Primate Somatosensory Cortex. Neuron. 2013; 78(6):1116–26. [PubMed: 23791200]
29. Logothetis NK, Pauls J, Augath M, Trinath T, Oeltermann A. Neurophysiological investigation of the basis of the fMRI signal. Nature. 2001; 412(6843):150–7. [PubMed: 11449264]
30. Logothetis NK. The underpinnings of the BOLD functional magnetic resonance imaging signal. J Neurosci. 2003; 23(10):3963–71. [PubMed: 12764080]
31. Kim T, Masamoto K, Fukuda M, Vazquez A, Kim SG. Frequency-dependent neural activity, CBF, and BOLD fMRI to somatosensory stimuli in isoflurane-anesthetized rats. Neuroimage. 2010; 52(1):224–33. [PubMed: 20350603]
32. Scholvinck ML, Maier A, Ye FQ, Duyn JH, Leopold DA. Neural basis of global resting-state fMRI activity. Proc Natl Acad Sci USA. 2010; 107(22):10238–43. [PubMed: 20439733]
33. Wilson GH 3rd, Yang PF, Gore JC, Chen LM. Correlated inter-regional variations in low frequency local field potentials and resting state BOLD signals within S1 cortex of monkeys. Hum Brain Mapp. 2016; 37(8):2755–66. [PubMed: 27091582]
34. Sur M, Nelson RJ, Kaas JH. Representations of the body surface in cortical areas 3b and 1 of squirrel monkeys: comparisons with other primates. J Comp Neurol. 1982; 211(2):177–92. [PubMed: 7174889]
35. Maier A, Wilke M, Aura C, Zhu C, Ye FQ, Leopold DA. Divergence of fMRI and neural signals in V1 during perceptual suppression in the awake monkey. Nat Neurosci. 2008; 11(10):1193–200. [PubMed: 18711393]
36. Shmuel A, Leopold DA. Neuronal correlates of spontaneous fluctuations in fMRI signals in monkey visual cortex: Implications for functional connectivity at rest. Hum Brain Mapp. 2008; 29(7):751–61. [PubMed: 18465799]

37. Manger PR, Woods TM, Munoz A, Jones EG. Hand/face border as a limiting boundary in the body representation in monkey somatosensory cortex. J Neurosci. 1997; 17(16):6338–51. [PubMed: 9236243]
38. Fang PC, Jain N, Kaas JH. Few intrinsic connections cross the hand-face border of area 3b of New World monkeys. J Comp Neurol. 2002; 454(3):310–9. [PubMed: 12442321]
39. Fame A, Roy AC, Giraux P, Dubernard JM, Sirigu A. Face or hand, not both: perceptual correlates of reafferentation in a former amputee. Curr Biol. 2002; 12(15):1342–6. [PubMed: 12176365]
40. Lu H, Zuo Y, Gu H, Waltz JA, Zhan W, Scholl CA, et al. Synchronized delta oscillations correlate with the resting-state functional MRI signal. Proc Natl Acad Sci U S A. 2007; 104(46):18265–9. [PubMed: 17991778]
41. Engel SA, Glover GH, Wandell BA. Retinotopic organization in human visual cortex and the spatial precision of functional MRI. Cereb Cortex. 1997; 7(2):181–92. [PubMed: 9087826]
42. Shi Z, Wu R, Yang PF, Chen LM, Gore JC. Functional connectivity within S1 cortex mapped by multi-channel LFPs: Comparisons with FMRI. Org Hum Brain Mapp. 2016; 22:4080.
43. Stoner R, Chow ML, Boyle MP, Sunkin SM, Mouton PR, Roy S, et al. Patches of disorganization in the neocortex of children with autism. N Engl J Med. 2014; 370(13):1209–19. [PubMed: 24670167]
44. Matsui T, Tamura K, Koyano KW, Takeuchi D, Adachi Y, Osada T, et al. Direct Comparison of Spontaneous Functional Connectivity and Effective Connectivity Measured by Intracortical Microstimulation: An fMRI Study in Macaque Monkeys. Cereb Cortex. 2011; 21(10):2348–56. [PubMed: 21368090]
45. Huber L, Goense J, Kennerley AJ, Trampel R, Guidi M, Reimer E, et al. Cortical lamina-dependent blood volume changes in human brain at 7 T. Neuroimage. 2015; 107:23–33. [PubMed: 25479018]
46. Baek K, Shim WH, Jeong J, Radhakrishnan H, Rosen BR, Boas D, et al. Layer-specific interhemispheric functional connectivity in the somatosensory cortex of rats: resting state electrophysiology and fMRI studies. Brain Struct Funct. 2016; 221(5):2801–15. [PubMed: 26077581]
47. Majumdar S, Wang F, Chen LM, Gore JC. High resolution fMRI reveals laminar specific resting-state functional connectivity in primary somatosensory cortex in nonhuman primates. Proc Int Soc Magn Reson Med. 2014; 22:4185.
48. Hutchison RM, Womelsdorf T, Allen EA, Bandettini PA, Calhoun VD, Corbetta M, et al. Dynamic functional connectivity: promise, issues, and interpretations. Neuroimage. 2013; 80:360–78. [PubMed: 23707587]
49. Chang C, Glover GH. Time-frequency dynamics of resting-state brain connectivity measured with fMRI. Neuroimage. 2010; 50(1):81–98. [PubMed: 20006716]
50. Shi Z, Rogers BP, Chen LM, Morgan VL, Mishra A, Wilkes DM, et al. Realistic models of apparent dynamic changes in resting-state connectivity in somatosensory cortex. Hum Brain Mapp. 2016; 37(11):3897–910. [PubMed: 27296233]
51. Wu TL, Mishra A, Wang F, Yang PF, Gore JC, Chen LM. Effects of isoflurane anesthesia on resting-state fMRI signals and functional connectivity within primary somatosensory cortex of monkeys. Brain Behav. 2016; 6(12):e00591. [PubMed: 28032008]
52. Yang PF, Wang F, Chen LM. Differential fMRI Activation Patterns to Noxious Heat and Tactile Stimuli in the Primate Spinal Cord. J Neurosci. 2015; 35(29):10493–502. [PubMed: 26203144]
53. Chen LM, Mishra A, Yang PF, Wang F, Gore JC. Injury alters intrinsic functional connectivity within the primate spinal cord. Proc Natl Acad Sci USA. 2015; 112(19):5991–6. [PubMed: 25902510]
54. Barry RL, Smith SA, Dula AN, Gore JC. Resting state functional connectivity in the human spinal cord. Elife. 2014; 3:e02812. [PubMed: 25097248]
55. Kong Y, Eippert F, Beckmann CF, Andersson J, Finsterbusch J, Buchel C, et al. Intrinsically organized resting state networks in the human spinal cord. Proc Natl Acad Sci U S A. 2014; 111(50):18067–72. [PubMed: 25472845]
56. Florence SL, Wall JT, Kaas JH. Central projections from the skin of the hand in squirrel monkeys. The Journal of comparative neurology. 1991; 311(4):563–78. [PubMed: 1721925]

57. Qi HX, Kaas JH, Reed JL. The reactivation of somatosensory cortex and behavioral recovery after sensory loss in mature primates. Front Syst Neurosci. 2014; 8:84. [PubMed: 24860443]
58. Chen LM, Qi HX, Kaas JH. Dynamic reorganization of digit representations in somatosensory cortex of nonhuman primates after spinal cord injury. J Neurosci. 2012; 32(42):14649–63. [PubMed: 23077051]
59. Qi HX, Gharbawie OA, Wynne KW, Kaas JH. Impairment and recovery of hand use after unilateral section of the dorsal columns of the spinal cord in squirrel monkeys. Behav Brain Res. 2013; 252:363–76. [PubMed: 23747607]
60. Yang PF, Qi HX, Kaas JH, Chen LM. Parallel functional reorganizations of somatosensory areas 3b and 1, and S2 following spinal cord injury in squirrel monkeys. J Neurosci. 2014; 34(28):9351–63. [PubMed: 25009268]
61. Reed JL, Liao CC, Qi HX, Kaas JH. Plasticity and Recovery After Dorsal Column Spinal Cord Injury in Nonhuman Primates. Journal of experimental neuroscience. 2016; 10(Suppl 1):11–21. [PubMed: 27578996]
62. Wu R, Su L, Yang PF, Min Chen L. Altered Spatiotemporal Dynamics of Cortical Activation to Tactile Stimuli in Somatosensory Area 3b and Area 1 of Monkeys after Spinal Cord Injury. eNeuro. 2016; 3(5)
63. Tettamanti M, Paulesu E, Scifo P, Maravita A, Fazio F, Perani D, et al. Interhemispheric transmission of visuomotor information in humans: fMRI evidence. J Neurophysiol. 2002; 88(2): 1051–8. [PubMed: 12163553]
64. Weber B, Treyer V, Oberholzer N, Jaermann T, Boesiger P, Brugger P, et al. Attention and interhemispheric transfer: a behavioral and fMRI study. J Cogn Neurosci. 2005; 17(1):113–23. [PubMed: 15701243]
65. Mazerolle EL, Beyea SD, Gawryluk JR, Brewer KD, Bowen CV, D'Arcy RC. Confirming white matter fMRI activation in the corpus callosum: co-localization with DTI tractography. Neuroimage. 2010; 50(2):616–21. [PubMed: 20053383]
66. Fabri M, Polonara G, Mascioli G, Salvolini U, Manzoni T. Topographical organization of human corpus callosum: an fMRI mapping study. Brain Res. 2011; 1370:99–111. [PubMed: 21081115]
67. Gawryluk JR, D'Arcy RC, Mazerolle EL, Brewer KD, Beyea SD. Functional mapping in the corpus callosum: a 4T fMRI study of white matter. Neuroimage. 2011; 54(1):10–5. [PubMed: 20643213]
68. Mazerolle EL, Gawryluk JR, Dillen KN, Patterson SA, Feindel KW, Beyea SD, et al. Sensitivity to white matter FMRI activation increases with field strength. PLoS One. 2013; 8(3):e58130. [PubMed: 23483983]
69. Nonaka H, Akima M, Hatori T, Nagayama T, Zhang Z, Ihara F. Microvasculature of the human cerebral white matter: arteries of the deep white matter. Neuropathology. 2003; 23(2):111–8. [PubMed: 12777099]
70. Nonaka H, Akima M, Hatori T, Nagayama T, Zhang Z, Ihara F. The microvasculature of the cerebral white matter: arteries of the subcortical white matter. J Neuropathol Exp Neurol. 2003; 62(2):154–61. [PubMed: 12578225]
71. Raichle ME, MacLeod AM, Snyder AZ, Powers WJ, Gusnard DA, Shulman GL. A default mode of brain function. Proc Natl Acad Sci USA. 2001; 98(2):676–82. [PubMed: 11209064]
72. Ding Z, Newton AT, Xu R, Anderson AW, Morgan VL, Gore JC. Spatio-temporal correlation tensors reveal functional structure in human brain. PLoS One. 2013; 8(12):e82107. [PubMed: 24339997]
73. Ding Z, Xu R, Bailey SK, Wu TL, Morgan VL, Cutting LE, et al. Visualizing functional pathways in the human brain using correlation tensors and magnetic resonance imaging. Magn Reson Imaging. 2016; 34(1):8–17. [PubMed: 26477562]
74. Wu TL, Wang F, Anderson AW, Chen LM, Ding Z, Gore JC. Effects of anesthesia on resting state BOLD signals in white matter of non-human primates. Magn Reson Imaging. 2016; 34(9):1235–41. [PubMed: 27451405]

Highlights

1. Low frequency correlations of resting state fMRI signals are a general feature of the neural system.
2. RsFC is strong between regions in the brain and spinal cord that are engaged in the same function.
3. At mesoscale, resting state correlation of fMRI signals correlate very well with electrophysiological signals and anatomical connections.

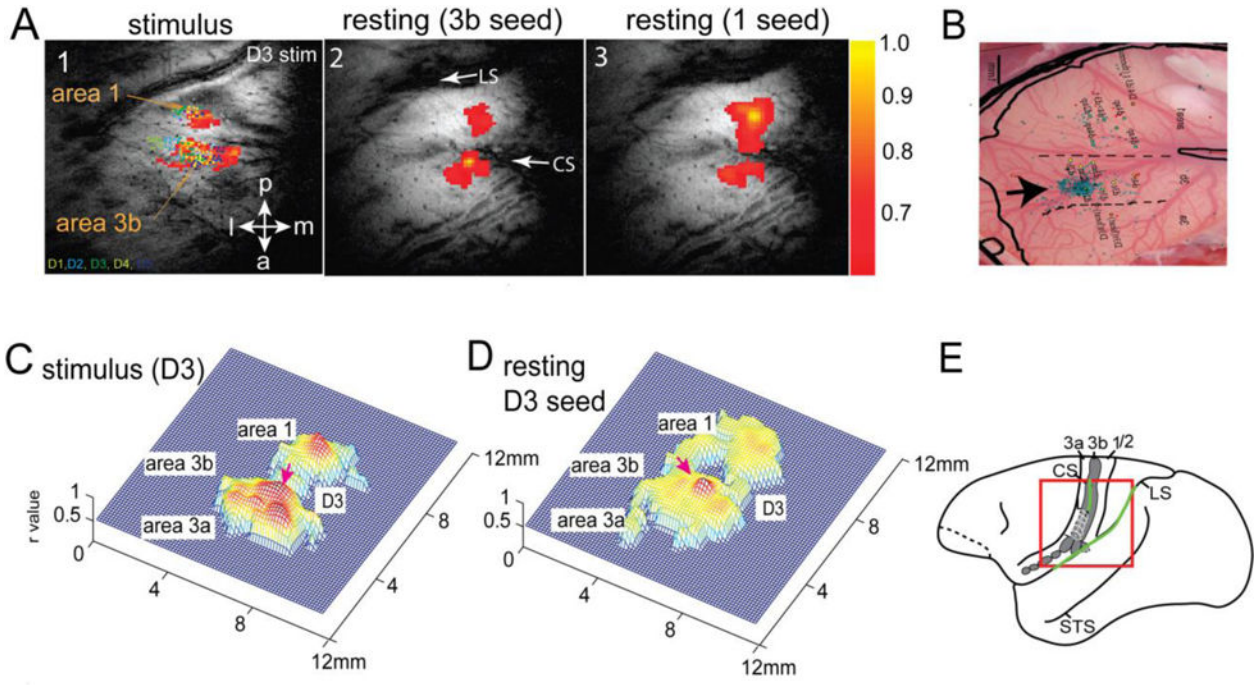

Figure 1.

Relationship between rs-FC and anatomical connection. (A1) BOLD activation map (resolution: 0.55×0.55×2mm^3) elicited by 8Hz vibrotactile stimulation of digit 3 (D3). Color dots represent the receptive field (D1–D5) and microelectrode recording sites. (A2–3) Correlation maps (thresholded at r = 0.6) of seeds (yellow voxels) identified at the centers of area 3b (2) and area 1 activation foci. (B) BDA (Biotinylated dextran amines) tracer injection in area 3b (black arrow). Light blue patches are BDA labeled terminals. Receptive fields were used to determine the digit region for injection. (C–D) 3D plots of A1 and A2. (E) Schematic illustration of the imaging field of view (redline box) and location of S1 subregions (areas 3a, 3b, 1/2) on squirrel monkey brain outline. CS/LS: central and lateral sulci; STS: superior temporal sulcus. Modified from (28).

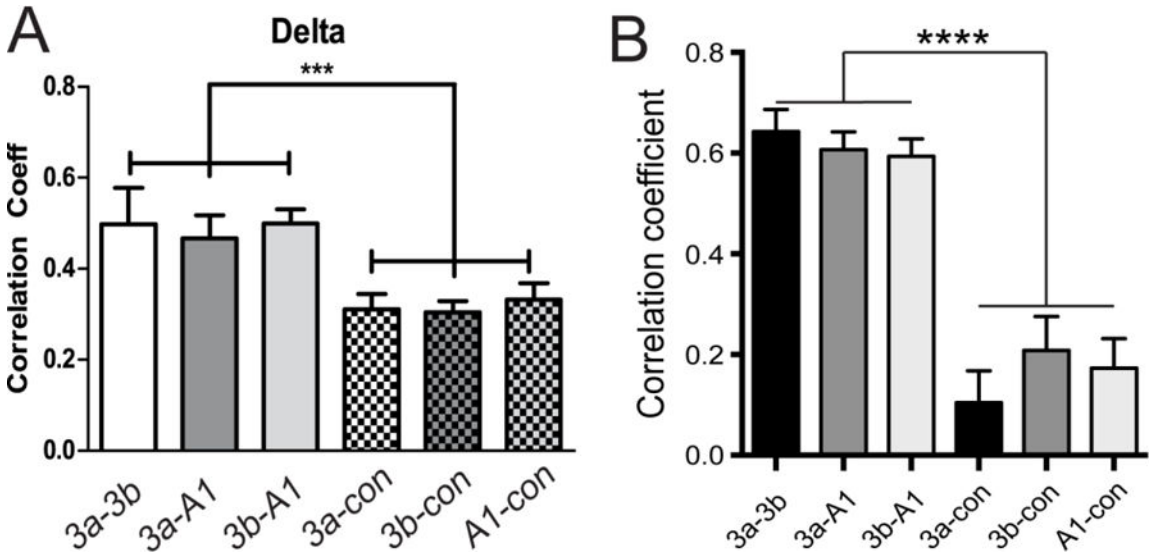

Figure 2.

Inter-areal rsfMRI connectivity covaries with inter-areal correlations of delta, alpha, and gamma low bands of LFP signals within S1 cortex. (A) Functional connectivity measures between sub-regions of digit representation within S1 (3a–3b, 3a–A1, 3b–A1) and between S1 digit and face control (3a-con, 3b-con, A1-con) region for delta band LFPs. (B) The same correlation pattern for rsfMRI signals. Modified from (33).

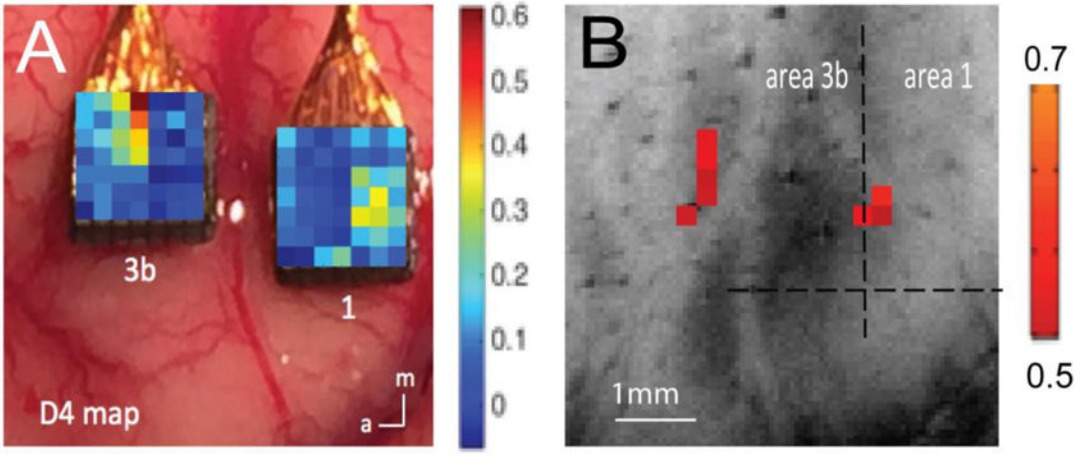

Figure 3.

Comparison of spatial profiles of BOLD and LFP signals to tactile stimulation. (A–B) Single digit tactile stimulation evoked LFP (A) and BOLD (B) responses (in % signal changes; see color bar for range) to tactile stimulation of digit 4 (D4). Modified from (42).

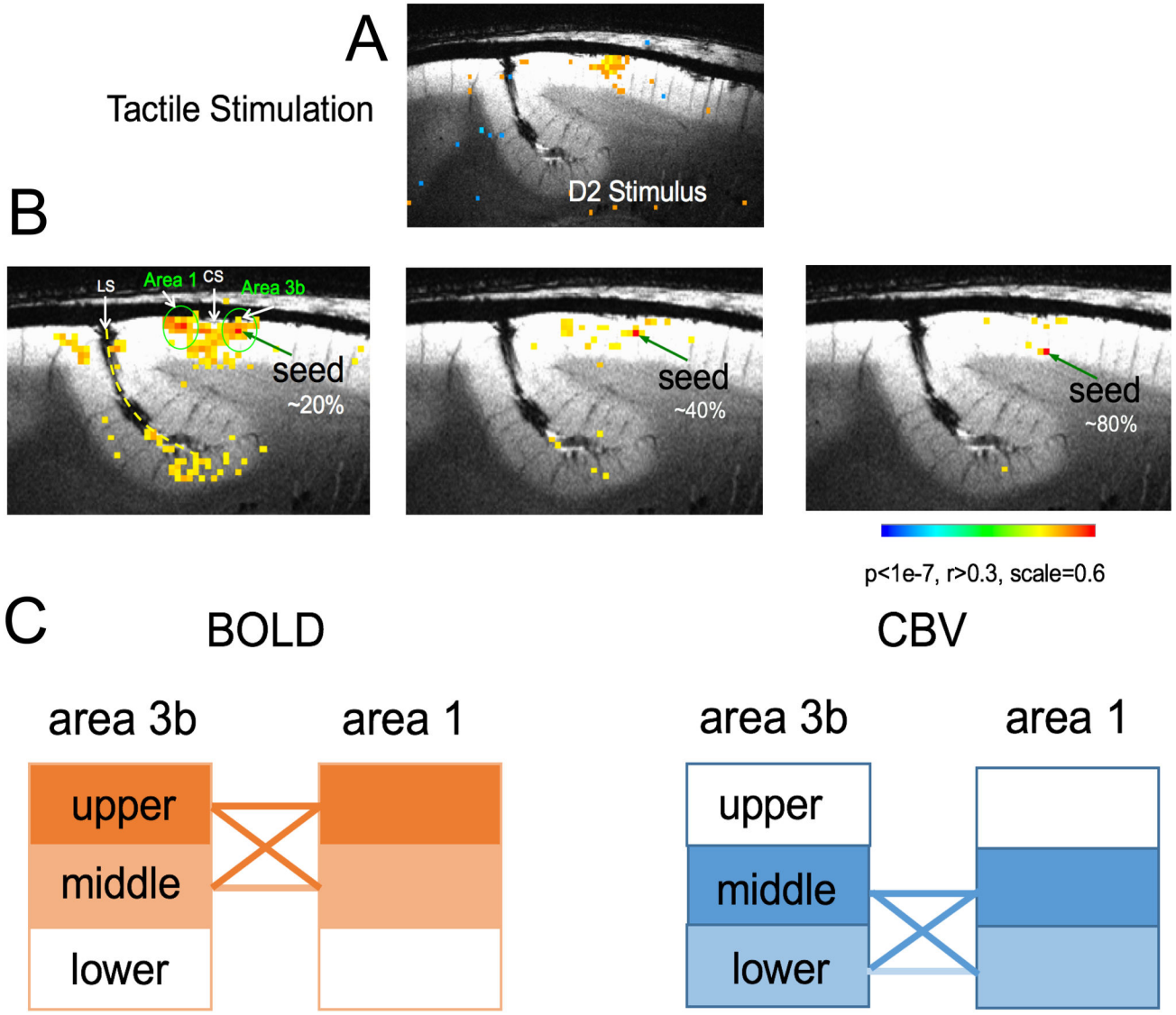

Figure 4.

Layer-specific resting state functional connectivity (rsFC) between areas 3b and 1. (A) Tactile stimulus-evoked BOLD activation map (thresholded at $t > 2.7$). (B) Voxel-wise BOLD correlation maps of seeds in upper, middle, and lower layers (depths) of area 3b. Correlation maps are thresholded at $r > 0.3$. (C) Schematic illustration of the differences between CBV and BOLD inter-layer functional connectivities. Solid lines indicate the functional connections between layers are strong and significant. Modified from (47).

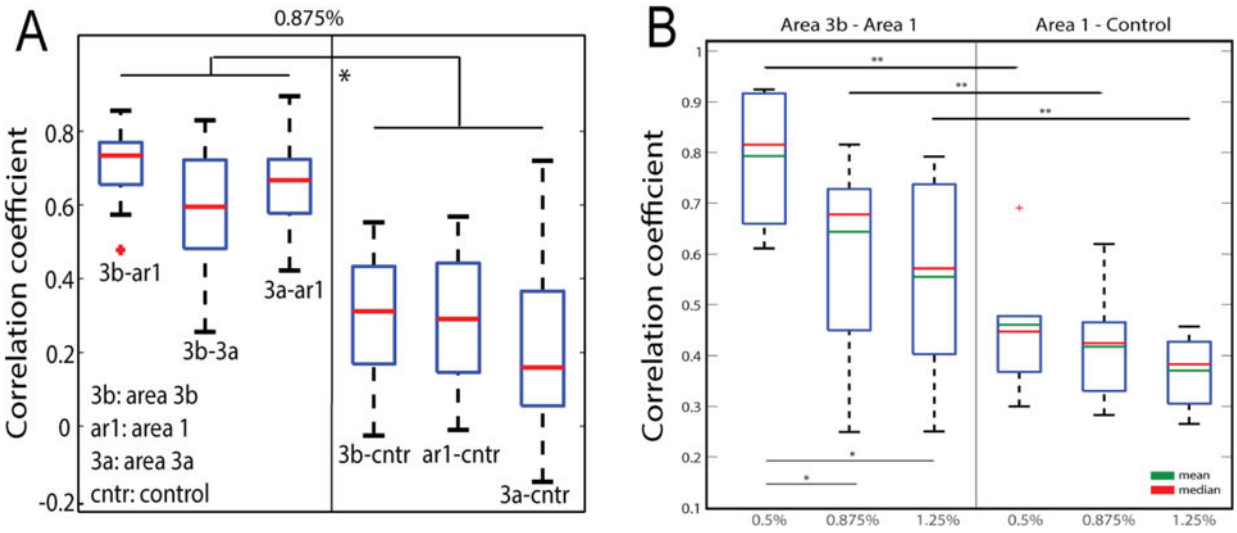

Figure 5.

Differential inter-areal functional connectivity of resting state BOLD signals between digit-digit (3b-ar1, 3b-3a, 3a-ar1) and digit-face control (3b-cntr, ar1-cntr, 3a-cntr) region pairs (A) and the effects of different doses of isoflurane on inter-areal rsfMRI BOLD connectivity (B). Modified from (51).

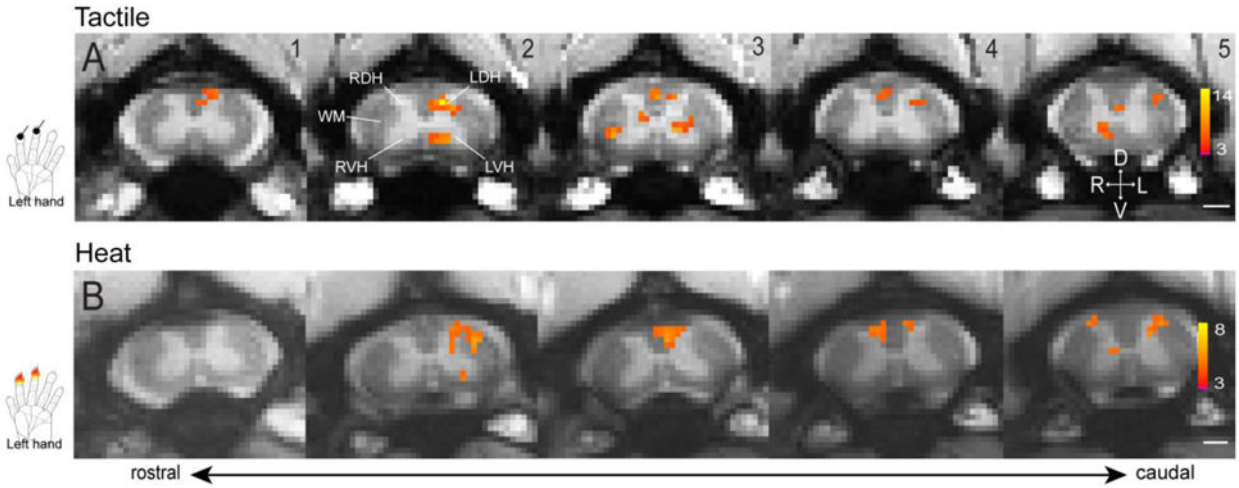

Figure 6.

Representative fMRI activations to tactile and nociceptive heat stimulation of two distal finger pads. (A) Multi-run average fMRI activations to tactile stimulation of two distal finger pads on left hand. (B) Multi-run average fMRI activations to 47.5 °C nociceptive heat stimulation of two distal finger pads on left hand. Hand inserts show the locations of stimulation. All activation maps are thresholded at $p < 0.05$ for multi-run with FDR (0.01) correction, see color scale bar on image 5 for the t value range. Images 1–5: from rostral to caudal. Scale bars indicate 1 mm. D: dorsal; V: ventral; L: left; R: right. Modified from (52).

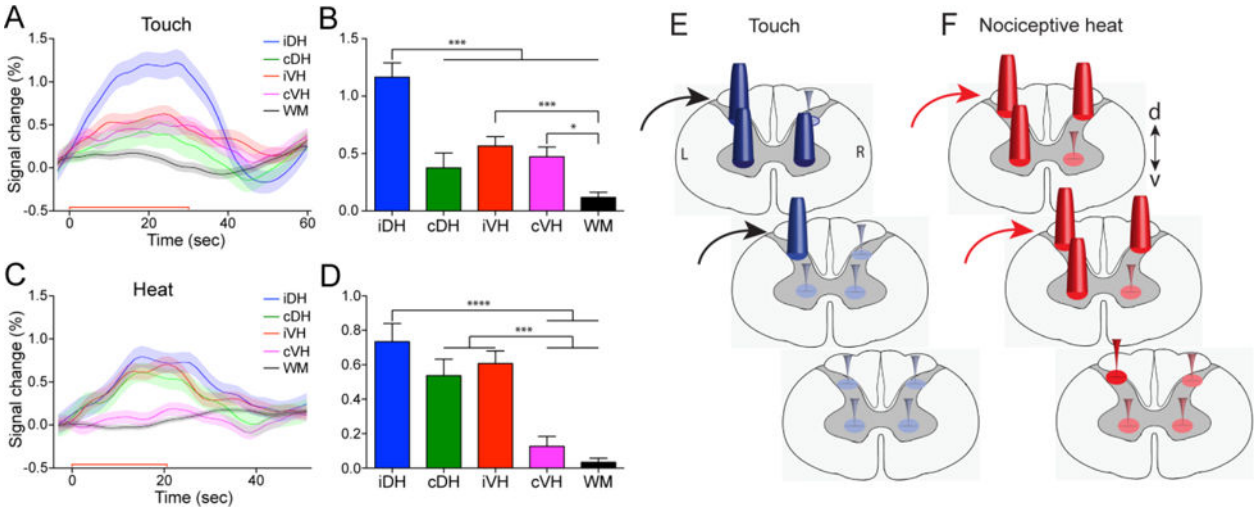

Figure 7.

Differential fMRI response magnitudes of four horns to touch versus nociceptive heat stimuli within a single spinal segment, and a schematic summary. (A, C) Time courses of fMRI signal changes to unilateral tactile (A) and nociceptive heat (C) stimulation of two distal finger pads in the iDH: ipsilateral dorsal horn; cDH: contralateral dorsal horn; iVH: ipsilateal ventral horn and cVH: contralateral ventral horn, and one white matter (WM) region. Color lines and shadows indicate mean ± standard error of the percentage fMRI signal changes. The red lines near the x-axis show the stimulation periods of 30 sec for tactile and 22 sec for heat, respectively. (B, D) Statistical comparisons of the group peak magnitudes of fMRI signal changes (mean ± standard error). *$p < 0.05$; *** $p < 0.005$; **** $p < 0.001$. (E, F). Schematic summarizing the differential activation patterns to touch (E) versus nociceptive heat (E) stimulation within and across (raw data not shown) spinal segments. Dark blue and red cones indicate responses are significant. Orange, green and magenta color cones indicate statistically different responses between touch and nociceptive heat. Modified from (52).

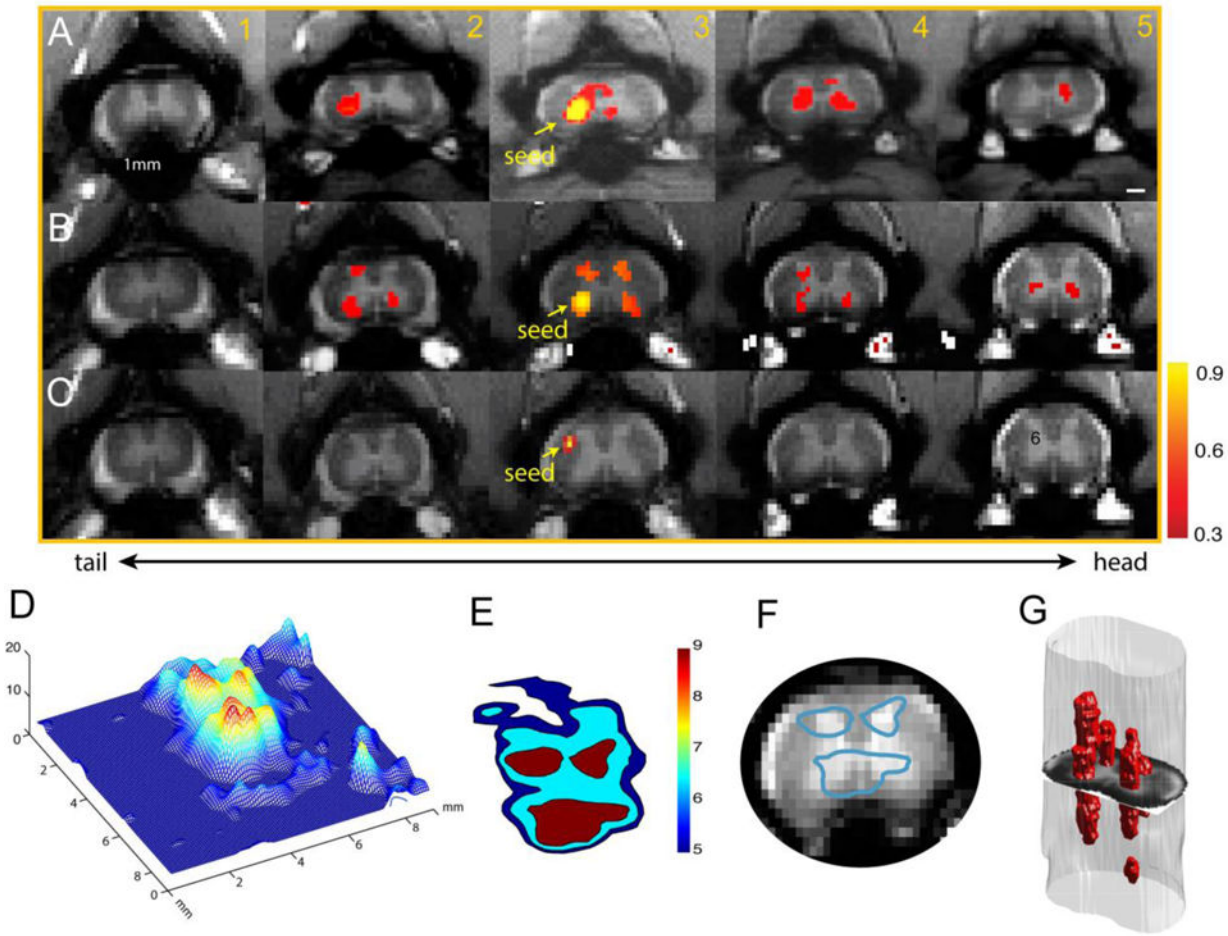

Figure 8.

Reproducible functional connectivity pattern of the spinal cord horns. (A & B) Intra-(within) and inter-(across) slice correlation patterns of the seeds (indicated by yellow arrows) placed at the ventral horns on slice 3 in two representative normal animals. Correlation maps were thresholded at $r > 0.30$ (see color scale bar next to image column 5). (C) Intra- and inter-slice correlation pattern of one control seed in the white matter. (D) 3-D illustration of the t-statistic of the correlation map of the right ventral horn at the group level (15 runs from 5 animals). (E) Corresponding contour map of the group correlation pattern at three different t-statistics (blue: t=5; light blue: t=6.5; red: t=9). The left ventral horn in slice 3 in one subject was used as the point of interest for manual co-registration in the group analysis. (F) Overlay of the thresholded (red patch) correlation map of left ventral horn seed on the mean intensity map of the spinal cord MTC images. (G) 3D reconstruction of the correlation map from the sample case shown in A. Adapted from (53).

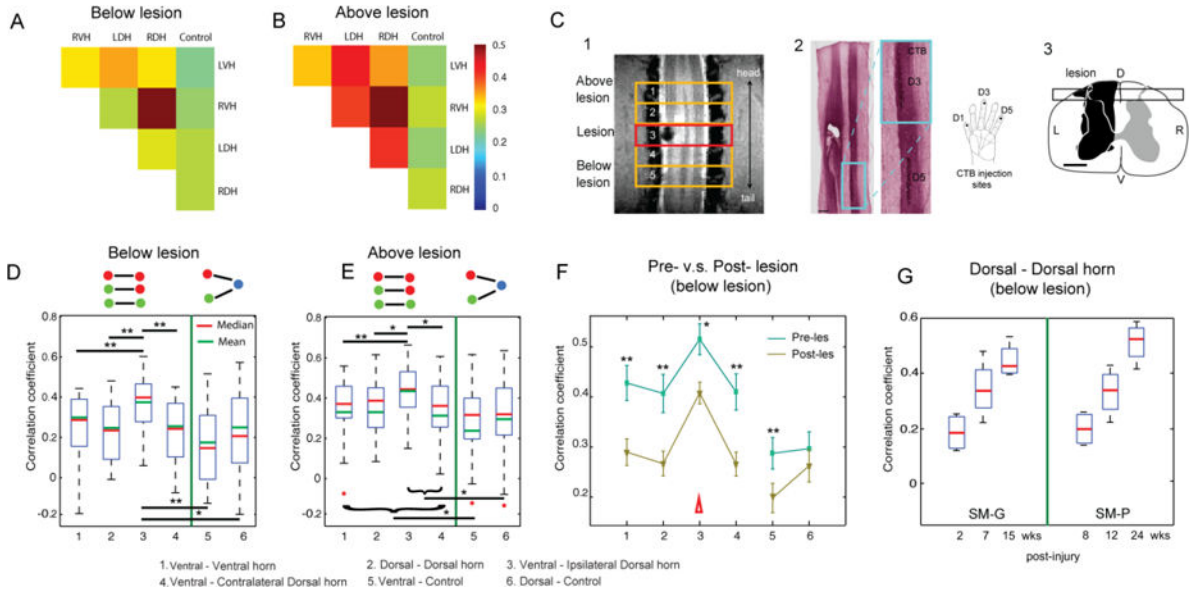

Figure 9.

Effects of a unilateral spinal cord lesion on the functional connectivity of intra-slice seed ROIs. (A and B) The 2D matrix plots of the mean correlation coefficients (r-values) among all five intra-slice ROI pairs in below (A) and above (B) lesion slices in one representative animal (SM-P). The color bar indicates the range of r-values. (C, 1) Coronal MTC image shows the actual lesion (black hole) detected at the 24-week post-lesion time point. Red rectangle outline shows the placement of the third axial image slice, which is centered at the lesion level. (C, 2) CTB stain of the corresponding postmortem spinal cord obtained at 24 weeks after the lesion. Zoomed-in image (left) shows the CTB terminals of the afferent entering zone for D5 and D3. (C, 3) The reconstructed lesion on the axial plane of the spinal cord in monkey SM-P. Black rectangle outline shows the location of the coronal MRI image shown in 2. (D and E) Whisker box plots of the correlation coefficients between horn-horn ROI (columns 1–4) and horn–control (white matter) ROI pairs (columns 5–6) at the imaging slices below lesion (slices 5 and 6) and above lesion (slices 1 and 2), respectively. Green lines separate the horn–horn and horn–control ROI pair groups. (F) Direct comparison of the mean correlation coefficients of the same set of ROI pairs obtained before (prelesion, green line) and after (postlesion, yellow line) the lesions. Error bars indicate the SD of the measurements. Datasets of 10 runs from two monkeys with spinal cord lesion acquired within 2–24 weeks postlesion were included in this analysis. (G) Whisker box plot of the correlation coefficients between dorsal-dorsal horns in below-lesion slices as a function of postlesion time point (in weeks) in two injured monkeys. Adapted from (53).

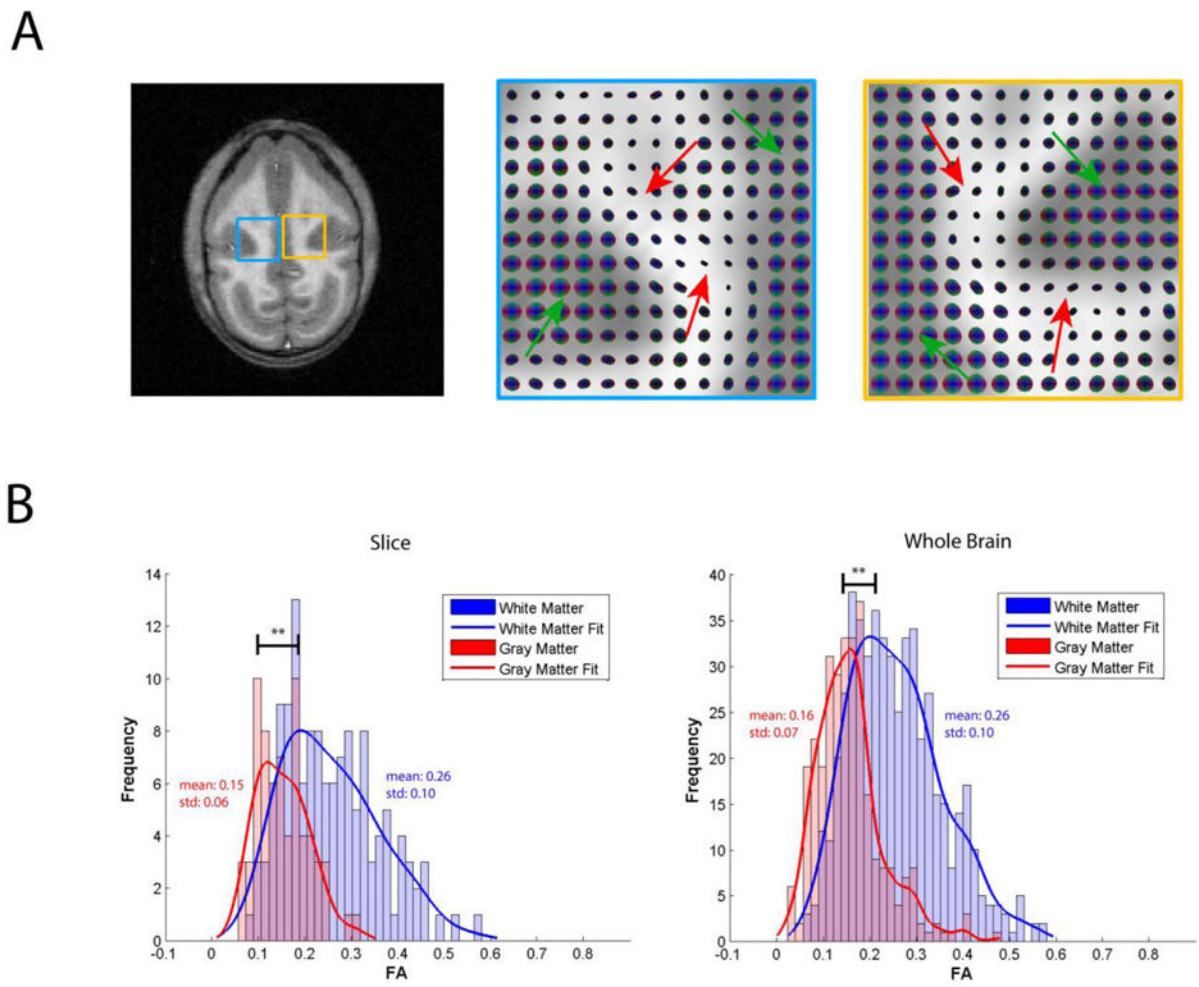

Figure 10.

(A) T_1-weighted anatomical image accompanied by enlarged spatio-temporal correlation tensor maps in the blue and yellow regions. Green arrows on tensor maps point to grey matter isotropic tensors, while red arrows point to white matter anisotropic tensors (B). Histograms of fractional anisotropy values for the tensors in the slice, as well as for the whole brain presented in (A). ** $p < 0.0005$ (Mann–Whitney Test). Adapted from (74).